Full Paper

Propellants, Explosives, Pyrotechnics

DOI: 10.1002/prep.201800290

Initiation and Overdriven Detonation of High Explosives Using Multipoint Initiation

Junfeng Guo,[a, b] Qingxuan Zeng,*[a, b] Guosheng Qin,[b] and Mingyu Li*[a]

In Memory of Michael Hiskey

Abstract: High explosives (HE) with desirable safety and detonation performances are widely used in weapon system and aerospace engineering. Multipoint initiation is utilized to initiate TATB and thus create overdriven state. High-pressure areas of colliding shock waves are observed by measuring steel dent value and the whole processes, involving multiple wave interactions and overdriven detonation formation, are reproduced using LS-DYNA3D program. Results indicate that the quadruple point is at the center where four shock waves collide, and the double point is between two initiation points where two shock waves collide. When the height of donor explosive exceeds 5 mm, the retardation time of the quadruple point compared to the double point and the individual point are 180 ns and 260 ns, respectively. In addition, overdriven state may disappear when the height of UF-TATB exceeds 9 mm, and the delay effect is negligible for initiating PBX-9502 when the simultaneity of slapper detonators is within 100 ns.

Keywords: Multipoint initiation · Interaction · Overdriven detonation · High explosive · Simultaneity

1 Introduction

Design of high explosives (HE) always requires higher safety and more desirable detonation performances, while it may need a larger booster to be initiated. 2,4,6 Triamino-1,3,5 Trinitro-Benzene (TATB) is set a standard for HE insensitivity and widely used in weapon system and aerospace engineering. Since the initiation of TATB is difficult, multipoint initiation atracts much atention as an initiating technology for HE.

Multipoint initiation could create multiple shock wave interactions and thus reach an elevated pressure at the center, which can be utilized to initiate insensitive HE, such as TATB. Gates [1] developed an initiation system for extremely insensitive detonating substance (EIDS). In this system, four grains were initiated simultaneously and subsequent shock wave interactions would occur at the center, which could initiate the EIDS. Subsequently, Cope and Gates [2–3] designed a MEMS in-situ detonator based on S&A device technology to ensure the simultaneity of multipoint initiation system. However, synergized initiation mechanisms and Mach stem evolution were rarely mentioned in their research. Tasker [4] designed a synergized initiation system where three grains were utilized to create triple CJ pressure at the center and high-density TATB can be initiated, while the measurement of triple pressure was not conducted in this research. Further, PDV was utilized to measure pressure output at various charge sizes and determine the detonation of explosives, which proved that the charge size is lower than that when using single point initiation [5]. Whilst, with the same charge quality, centre pressures of three-point, four-point, six-point and eight-point were measured by a Manganese Bronze manometry [6]. Results show that the four-point initiation system can achieve much higher pressure. But more information, such as the growth, propagation and interaction of shock waves and duration of overdriven state, can hardly be observed experimentally. To undestand the synergized initiation mechanisms, there is still a great challenge in how to reproducing the whole processes.

In this work, LS-DYNA3D program is utilized to reproduce the whole processes involving multiple shock waves interaction beween donor explosives and the formation and longvity of overdriven detonation in acceptor explosives. The 3D model hepls to understand the initiation mechanisms and optimize charge structure. Meanwhile, the values of steel dent and central pressure are measured compared with simulation results.

[a] *J. Guo, Q. Zeng, M. Li*
State Key Laboratory of Explosion Science and Technology
Beijing Institute of Technology
Beijing, China
**e-mail: zengqingxuan@bit.edu.cn*
mingyuli@163.com
[b] *J. Guo, Q. Zeng, G. Qin*
National Key Laboratory of Applied Physics and Chemistry
Shaanxi Applied Physics and Chemistry Research Institute
xi'an, China

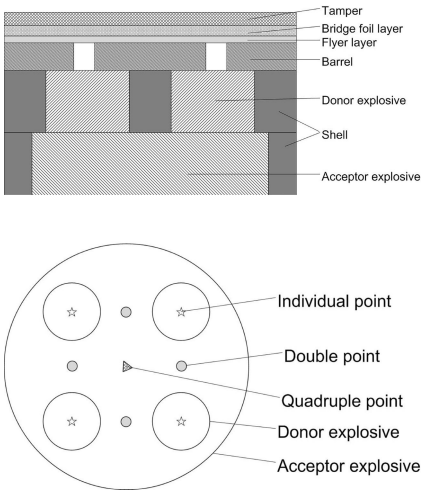

Figure 1. Schematic of a four-point initiation system (up: axial profile view; down: top view).

2 Numerical Approach

As usual, a multipoint initiation system can be mainly divided into three parts: (1) slapper detonator array, (2) donor explosive array; (3) acceptor explosive. A slapper detonator, with no primary explosive, consists of tamper, bridge foil, flyer and barrel. Owing to its high safety and simultaneity, slapper detonator array, as often, is utilized to simultaneously initiate donor explosive array and thus create shock wave interactions. Then a large-scale acceptor explosive can be initiated and overdriven detonation may be created. Figure 1 shows schematic of a four-point initiation system in the axial profile view (up) and the top view (down).

Since a slapper detonator has the performances of small-scale size and short duration, initiation points are utilized instead of slapper detonators in this model. When donor explosives are initiated instantaneously by the slapper detonators, shock wave interactions occur between donor explosives and thus ultra-high pressures can be created. As for the four-point initiation system, the quadruple point is at the center where four shock waves collide and the double point is between two initiation points where two shock waves collide. The individual point is below the initiation point where a detonation wave is propagated in donor explosives.

To understand the synergized initiation mechanism, LS-DYNA3D program is employed to reproduce the whole processes. In this model, high explosive burn model and JWL equation of state (EOS) is chosen to reflect growth and propagation of detonation waves in donor explosives. Donor explosive is HNS with the density of 1.6 g cm^{-3} in this case. Detonation velocity and CJ pressure of HNS were measured as 6800 m s^{-1} and 18.7 GPa at this density, respectively [7]. JWL EOS can be expressed as

$$P = A\left(1 - \frac{\omega}{R_1 V}\right)e^{-R_1 V} + B\left(1 - \frac{\omega}{R_2 V}\right)e^{-R_2 V} + \frac{\omega E}{V} \quad (1)$$

where P is pressure; V is relative volume; E is internal energy; A, B, R_1, R_2 and ω are constant [8]. Parameters of JWL EOS for 1.6 g cm^{-3} HNS can be described as: $A = 536.25$ GPa, $B = 27.02$ GPa, $R_1 = 5.4$, $R_2 = 1.8$ and $\omega = 0.45$ [9].

To analyze the initiation mechanism, two TATB explosives, one for UF-TATB (pure ultra-fine TATB) with the density of 1.8 g cm^{-3} and one for PBX-9502 (TATB/Kel-F = 95 : 5) with the density of 1.895 g cm^{-3}, are employed as acceptor explosives. Reaction zone length of TATB is about 0.3 mm [10]. The Ignition and Growth reactive flow model is employed to reflect detonation wave changes during the acceptor. This model consists of two JWL EOS's, one for unreacted explosive and one for detonation product, and one three-term reaction rate equation. The reaction rate equation can be expressed as

$$\frac{d\lambda}{dt} = I(1-\lambda)^b\left(\frac{\rho}{\rho_0} - 1 - a\right)^x + G_1(1-\lambda)^c\lambda^d P^y + G_2(1-\lambda)^e\lambda^g P^z \quad (2)$$

where λ is reaction rate; t is time; ρ_0 and ρ are initial density and product density, relatively; I, G_1, G_2, a, b, c, d, e, g, x, y and z are constant [8]. Detailed parameters of the Ignition and Growth reactive flow model for TATB with the density of 1.8 g cm^{-3} and 1.895 g/cm^3 are listed in literature [11].

The whole processes, involving of the growth, propagation and interaction of shock waves, Mach steam evolution and longevity of overdriven state, can be reproduced using the 3D model, which helps to understand the synergized initiation mechanisms. In addition, the influence of the size of the donor on quadruple pressure and the simultaneity of slapper detonators on the initiation of TATB are conducted via the simulations, which helps to optimize the design of multipoint initiation system. However, more effects are made to modify parameters of EOS for improving the precision of the model.

3 Numerical Simulation and Comparison

To observe high-pressure areas of the donor, witness boards are placed at the bottom of donor explosives instead of acceptor explosives. The material of witness boards is No. 20 cold drawn steel. Thus, high-pressure area can be observed by measuring the value of steel dents. Meanwhile, the growth, propagation and interaction of shock waves are reproduced via the simulation, which helps to have a deeper understanding of the initiation mechanisms. Figure 2 shows the steel dent experiments for donor explosives with the center distance of 4 mm (left) and 8 mm (right). In these ex-

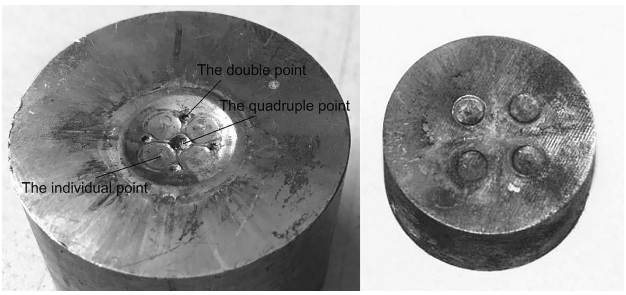

Figure 2. Steel dent experiments for donor explosives (left: with 4 mm center distance; right: with 8 mm center distance).

periments, the donor is four Φ 4 × 6 mm HNS grains which are instantaneously initiated by slapper detonators.

From Figure 2, we can see that steel dent value for 4 mm center distance is much deeper than that for 8 mm center distance. Experimental results indicate that smaller center distance can create much higher pressure at the center. This is because air damping effect increases with center distance increasing. Meanwhile, the quadruple point is at the center where four shock waves collide, and the double point is between initiation points where two shock waves collide. When the center distance is 4 mm, the values of steel dents for the quadruple point and the individual point are measured as 1.02 mm and 0.32 mm, respectively. That indicates that shock wave interactions occur at the center and the central pressure can reach a few times CJ pressure. However, more information, such as how long the high-pressure points arrive the bottom of the donor and how much the pressures can reach, are not known in these experiments.

To have a deeper understanding of the initiation mechanism, the simulations are conducted using the LS-DYNA3D program. Figure 3 shows an axial profile view for the shock wave interaction simulation at 0.89 μs when the center distance is 4 mm. In Figure 3, the bar represents the pressure levels at Mbar, and the arrow shows the direction of the detonation.

From Figure 3, we can see that the quadruple point may be located at the center while that is behind the double point and the individual point. That is because a double point is produced by two adjacent individual shock waves

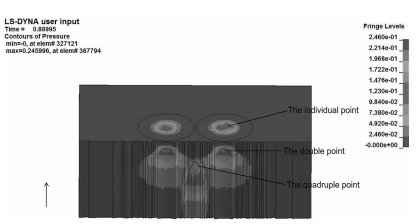

Figure 3. Axial profile view for shock wave interaction simulation at 0.89 μs.

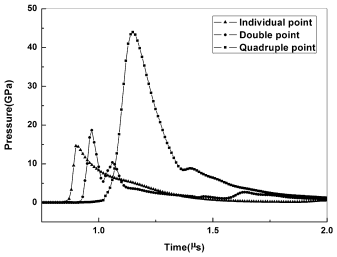

Figure 4. Pressure curves of the individual, double and quadruple points.

and then the quadruple point may be produced by the coupling of double shock waves and individual shock waves. Figure 4 shows the pressure curves of the individual, double and quadruple points at the bottom of the donor when the center distance is 4 mm.

From Figure 4, we can see that quadruple pressure (44.0 GPa) is much higher than individual pressure (14.6 GPa) and double pressure (18.7 GPa) while the quadruple point falls behind the double point and the individual point in turn. In this case, the retardation time of the quadruple point compared to the double point and the individual point are 180 ns and 250 ns, respectively. Since the initiation of acceptor explosives is determined by the critical initiation pressure, initiation mechanisms may be various. When the sensitivity of acceptor explosive is high, the acceptor can be initiated by an individual point. When the sensitivity is lower, it may be initiated by the double point. When the sensitivity is comparatively low, it only can be initiated by the quadruple point.

Further, the simulation is conducted when the center distance is 8 mm. As for the arrival time, the similar law is shown. However, quadruple pressure is only 5.4 GPa in this case, which is much lower than indivdual pressure. That can explain that there is no obvious steel dent at the quadruple point when the center distance is 8 mm.

To determine the initiation of acceptor explosive, a No. 20 cold drawn steel board is placed at the bottom of the acceptor. In this experiment, the acceptor is Φ 15 × 14.3 mm UF-TATB. Figure 5 shows the steel dent experiment for UF-TATB when the center distance of donor explosives is 4 mm.

From Figure 5, we can see that there is an obvious steel dent at the center and the value of steel dent is measured as 1.83 mm. That indicates that UF-TATB is initiated when the center distance is 4 mm. However, initiation mechanism of UF-TATB is unclear. The simulation is conducted and the results of central pressures at various detonation depths for UF-TATB are shown in Figure 6.

From Figure 6, we can see that the maximum of central pressure firstly increases, then decreases, and eventually tends to CJ pressure (~31 GPa). When detonation depth exceeds 9 mm, the overdriven state of UF-TATB disappears. That is because the sensitivity of UF-TATB is as high that UF-TATB can be initiated by individual or double points other

Figure 5. Steel dent experiment for UF-TATB.

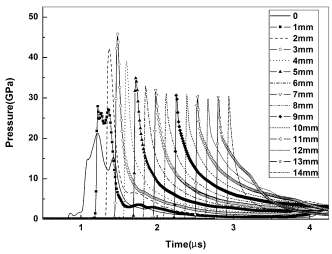

Figure 6. Central Pressures at various detonation depths for UF-TATB.

than quadruple points. Thus, in the initial stage centre pressures may increase and reach an ultra-high value (overdriven state) due to multiple detonation wave interactions, and then central pressures may decrease to CJ pressure with the detonation depth increasing. Steel dent experiments provide an approach to observe the high-pressure areas, but more efforts should be made to study the relationship of pressures with steel dents for various explosives.

To verify the rationality of the 3D model, the simulation results of quadruple pressures are compared with the experimental data. In their experiment [6], four HNS grains with the size of Φ 4 × 9 mm is instanously initiated by four slapper detonators and quadruple pressures are measured by the Manganese Bronze manometry. Table 1 is the comparison of experimental results of quadruple pressure with simulation results when center distance are 4 mm and 8 mm. From Table 1, we can see that simulation results are

Table 1. Comparison of experimental results of quadruple pressure with simulation results.

Center distance (mm)	Experimental data (GPa)[6]	Simulation results (GPa)	Relative error
4	47.2	49.9	5.7 %
4	48.7	49.9	2.4 %
8	13.7	14.0	2.3 %

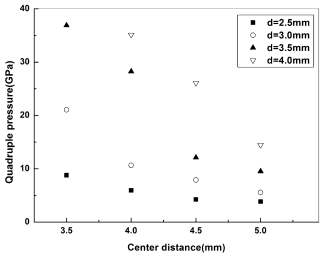

Figure 7. Quadruple pressures vs. center distance and charge diameters in air.

slightly higher than experimental results and the relative errors are within 6 %. Thus, the whole processes can be reproduced using LS-DYNA3D program, which can provide an approach to understand the synergized initiation mechanism and optimize the structure parameters of the system.

4 Discussion

The initiation ability of the multipoint system highly depends on the structure parameters of the donor. When the structure parameters are reasonable, central pressure can achieve a few times CJ pressure. Thus, as for the four-point initiation system, studying the influence of structure parameters on quadruple pressure is of great significance. Figure 7 shows the relationship of quadruple pressures with center distance and charge diameter (d) in air. Here, the charge height (H) is 4 mm.

From Figure 7, we can see that quadruple pressure increases with center distance decreasing or charge diameter increasing. The smaller the gap is, the higher the pressure can reach. To study the influence of charge height on shock wave interaction, charge diameter and center distance are determined as 4 mm. Table 2 is the relationship of pressure and arrival time with charge height in air.

From Table 2, we can see that with the charge height increasing, individual pressures and quadruple pressures continue to increase while double pressure changes are irregular. In this model, a very small air gap between two adjacent

Table 2. Pressures and arrival time vs. charge height in air.

H (mm)	P_{qua} [a] (GPa)	t_{qua} [a] (μs)	P_{dou} [b] (GPa)	t_{dou} [b] (μs)	P_{ind} [c] (GPa)	t_{ind} [c] (μs)
2	19.7	0.62	14.0	0.45	11.6	0.31
3	24.8	0.79	19.5	0.57	13.5	0.46
4	35.1	0.86	15.7	0.70	13.8	0.61
5	41.9	1.01	14.4	0.83	14.1	0.75
6	44.0	1.15	18.6	0.97	14.6	0.90
9	49.9	1.59	15.7	1.40	15.2	1.32

a) The subscript 'qua' is the value of quadruple point. b) The subscript 'dou' is the value of double point. c) The subscript 'ind' is the value of individual point.

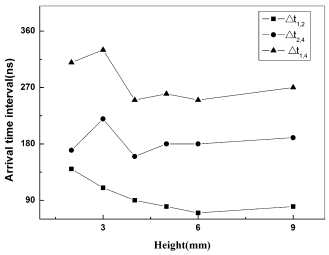

Figure 8. Arrival time interval vs. charge height in air.

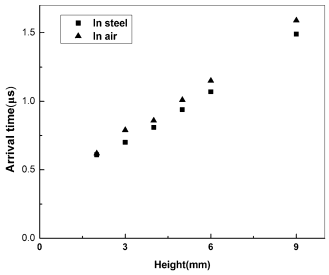

Figure 10. Arrival time of quadruple point vs. the height in air and in steel.

donor explosives is taken into account. Thus, double pressure may increase due to shock wave interactions and decrease due to air damping effect. Meanwhile, quadruple pressures are much higher than individual pressures, while double pressures are slightly higher than individual pressures. In addition, the quadruple point falls behind the double point and the individual point in turn. Figure 8 shows the relationship of the arrival time interval with the charge height in air. In Figure 8, the symbols Δt represents the arrival time interval, and the subscript '1, 2 and 4' represents the value of individual point, double point and quadruple point, respectively.

From Figure 8, we can see that $\Delta t_{1,2}$ continues to decrease while the changes of $\Delta t_{2,4}$ and $\Delta t_{1,4}$ are irregular when the charge height is lower than 5 mm. However, the arrival time intervals tends to a steady value when the height exceeds 5 mm. Here, the retardation time of the quadruple point compared with the double point and the individual point are 180 ns and 260 ns, respectively.

Meanwhile, the simulations in stainless steel are conducted to study the influence of the constraint material on shock wave interactions. Figure 9 shows the relationship of quadruple pressure with charge height in air and in stainless steel. Here, charge diameter and center distance are determined as 4 mm. From Figure 9, we can see that the law of pressure change in stainless steel is similar with that in air while quadruple pressures in stainless steel are much higher than that in air. That indicates that shock wave interactions in stainless steel can create an much higher pressure at the center compared with in air.

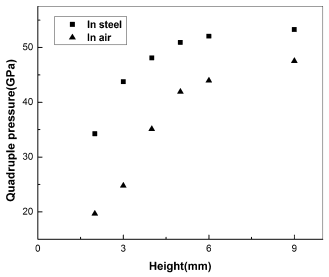

Figure 9. Quadruple pressure vs. the height in air and in steel.

Figure 10 shows the relationship of the arrival time of the quadruple point with charge height in air and in stainless steel. From Figure 10, we can see that the arrival time in stainless steel is slightly longer than that in air and the time intervel increases with charge height increasing. As usual, the closer shock impedance of constraint is to that of explosive, the weaker the reflection effect is. Thus, we will pay much attention to pursuing the constraint material in the next stage.

To study the influence of the simultaneity of slapper detonators on shock wave interaction, the four-point initiation system should satisfy the requirements that individual HNS grain is incapcable of initiating the acceptor but surmised four grains can. Thus, minimum priming charge size is required to be determined. Here, more insensitive PBX-9502 is chosen as acceptor explosive instead of UF-TATB. The size of PBX-9502 is Φ 15 $\times$ 14.3 mm, and the donor is the single-point or four-point HNS in stainless steel. Table 3 is the simulation results for HNS initiating PBX-9502.

From Table 3, we can see that the marginal size for single-point HNS is Φ 8 $\times$ 9 mm. Thus, the size of the individual HNS grain in the four-point initiation system is determined as Φ 4 $\times$ 8 mm. In this system, PBX-9502 is initiated by the quadruple point other than the individual or double point, and the charge quality of the donor is lower than the minimum priming charge quality. That indicates that multipoint initiation can reduce charge quality of the donor compared with single-point initiation.

Table 4 shows the simulation results at various delay times. Here, single-point delay is only taken into account.

Table 3. Simulation results for HNS initiating PBX-9502.

Diameter (mm)	Height (mm)	Quantiy	Type	Result
4	8	1	Single-point	No go
6	8	1	Single-point	No go
6	10	1	Single-point	No go
8	8	1	Single-point	No go
8	9	1	Single-point	Go
8	10	1	Single-point	Go
4	6	4	Four-point	No go
4	8	4	Four-point	Go

From Table 4, we can see that PBX-9502 can be initiated when the delay time is lower than 100 ns while cannot when the delay time exceeds 150 ns. That is, the delay effect can be negligible for initiating PBX-9502 when the simultaneity of slapper detonators is within 100 ns.

5 Conclusions

Multipoint initiation can create ultra-high pressure at the center using shock wave interactions, which can be utilized to initiate insensitive HE. Compared with single-point initiation, multipoint initiation does reduce the size of boosters. Actually, experimental characterization is extremely little other than pressure measurement at the edge and bottom. Thus, the growth, propagation and interaction of shock waves can hardly be observed experimentally. The 3D model can provide an approach to have a full understanding of the initiation mechanisms.

When acceptor explosives are initiated by colliding shock waves, the overdriven state starts to be created. However, the state may disappear when the height of acceptor explosives exceeds the threshold value. As for UF-TATB, the threshold value is 9 mm. Simulation results indicate that ultra-high pressure may appear at the center where four shock waves collide. When the height of donor explosive exceeds 5 mm, the retardation time of the quadruple point compared to the double point and the individual point are 180 ns and 260 ns, respectively. In addition, the four-point initiation system could initiate PBX-9502 when the delay time is lower than 100 ns while it fails to initiate when the delay time exceeds 150 ns.

Abbreviations

P Pressure
V Relative volume
E Internal energy
λ Reaction rate
t Time
ρ_0 Initial density
ρ Product density
d Charge diameter for donor explosive
H Charge height for donor explosive
P_{qua} Pressure at the quadruple point
P_{dou} Pressure at the double point
P_{ind} Pressure at the individual point
t_{qua} Arrival time at the quadruple point
t_{dou} Arrival time at the double point
t_{ind} Arrival time at the individual point
$\Delta t_{1,2}$ Arrival time interval between individual point and double point
$\Delta t_{2,4}$ Arrival time interval between double point and quadruple point

Table 4. Simulation results at various delay times.

Size (mm)	Type	Delay time (ns)	Delay quantity	Result
Φ 4×8	Four-point	50	1	Go
Φ 4×8	Four-point	100	1	Go
Φ 4×8	Four-point	150	1	No go
Φ 4×8	Four-point	200	1	No go

$\Delta t_{1,4}$ Arrival time interval between individual point and quadruple point

Acknowledgements

The authors thank many researchers at State Key Laboratory of Explosion Science and Technology and National Key Laboratory of Applied Physics and Chemistry for their works and ideas. This work is supported by the National Natural Science Foundation of China (11872013).

References

[1] R. Gates, US Navy Overview, *52th Annual Fuze Conference*, Sparks, NV, USA, **2008**.
[2] R. Cope, US Navy Overview, *53th Annual Fuze Conference*, Lake Buena Vista, FL, USA, **2009**.
[3] R. Gates, US Navy Overview, *54th Annual Fuze Conference*, Kansas City, Mo, USA, **2010**.
[4] D. G. Tasker, *Multipoint/Overdrive: Synergized Initiation Mechanisms.* No. LA-UR-17-22433. Los Alamos National Lab.(LANL), Los Alamos, NM (United States), **2017**.
[5] E. Francois, D. Tasker, R. Burritt, et al., Initiation of Insensitive High Explosives Using Multiple Wave Interactions, *AIP Conference Proceedings.* AIP Publishing, **2018**, 1979, 160009.
[6] K. H. Han, X. Ren, H. Li, et al., Simulation and Experimental Studies on the Multi-point Synchronization Detonation Overpressure of Slapper Detonators, *Chinese Journal of Energetic Materials.* **2016**, *24*, 38–44.
[7] M. L. Hobbs, M. R. Baer, Calibrating the BKW-EOS with a large product species database and measured CJ properties, *Tenth Symposium (International) on Detonation*, Boston, MA, **1993**.
[8] Manual, L. D. K. U. S., *Livermore Software Technology Corporation*, **2003**. *Version970*, 1088–1093.
[9] C. M Tarver, S. K. Chidester, Ignition and growth modeling of short pulse shock initiation experiments on fine particle hexanitrostilbene (HNS), *Journal of Physics: Conference Series* **2014**, *500*, 052044.
[10] A. Frank, H. Chau, R. Lee, et al., Reaction zones in ultrafine TATB, *Propellants*, *Explosives*, *Pyrotechnics.* **2003**, *28*, 259–264.
[11] C. M. Tarver, Modeling detonation experiments on triaminotrinitrobenzene (TATB)-based explosives LX-17, PBX 9502, and ultrafine TATB, *Journal of Energetic Materials.* **2012**, *30*, 220–251.

Manuscript received: September 25, 2018
Revised manuscript received: December 5, 2018
Version of record online: February 22, 2019

